ISSN 2616-5880 Vol. 6, Issue 3: 30-37, DOI: 10.25236/AJMC.2025.060303

Preparation and Electrochemical Properties of B-Doped $Na_4Fe_3(PO_4)_2(P_2O_7)$ Materials

Huayu Feng[a], Tingjun Song[b], Xinrui Xiao[c], Ling Chen[d,*]

School of Materials and Environment, Guangxi Minzu University, Nanning, Guangxi, China
[a]2961144503@qq.com, [b]sontinjn@foxmail.com, [c]18179621587@163.com, [d]chenlinggx@gxmzu.edu.cn
**Corresponding author*

Abstract: *The phosphate polyanionic $Na_4Fe_3(PO_4)_2(P_2O_7)$ cathode material stands out among many sodium ion battery cathode materials due to its stable structure, high safety and excellent sodium storage performance. However, the unsatisfactory conductivity and energy density limit its application. In this paper, the $Na_4Fe_3(PO_4)_2(P_2O_7)$ cathode material is doped with B element. The small-sized BO_3^{3-} doping replaces the PO_4^{3-} in the NFPP material will cause local lattice shrinkage, which can buffer the volume change during charging and discharging. The stability of the three-dimensional framework is optimized, thereby improving the electrochemical performance of the material. The results show that the appropriate amount of B doping can improve the reversible specific capacity of $Na_4Fe_3(PO_4)_2(P_2O_7)$ material, and improve the rate performance and cycle performance of the material. The NFPP-B0.05/C material has the best electrochemical performance, and the discharge specific capacity reaches 100.9 mAh g^{-1} at 0.2 C. At an ultra-high rate of 20 C, the discharge specific capacity of 84.1 mAh g^{-1} is still maintained, and the capacity retention rate is 92.6% after 1000 cycles at a high rate of 5 C.*

Keywords: *Sodium Ion Battery; Cathode Material; $Na_4Fe_3(PO_4)_2(P_2O_7)$; Electrochemical Performance*

1. Introduction

Olivine-type $LiFePO_4$ has been widely used in lithium-ion batteries. Iron-based polyanion compounds have become a research hotspot of cathode materials for sodium ion batteries due to their low cost, excellent structural stability and high safety[1]. Olivine-type $NaFePO_4$ has a high reversible capacity of 142 mAh g^{-1} and an average discharge voltage of 2.8 V[2]. However, unlike $LiFePO_4$, olivine-type $NaFePO_4$ cannot be directly prepared by traditional solid-state routes, but can only be prepared by chemical / electrochemical sodium ion insertion into heterogeneous $FePO_4$ or ion exchange routes, which will greatly increase production costs[3]. In addition, due to the large volume change of up to 17.58 % during the charge-discharge process, the olivine-type $NaFePO_4$ material exhibits poor cycle stability, which limits its practical application[4]. Although the $NaFePO_4$ material can be synthesized by the traditional solid phase method, the lack of effective sodium ion migration channels in its crystal structure limits the electrochemical performance and makes it difficult to meet the application requirements of sodium ion batteries[5]. As a derivative of $NaFePO_4$, $Na_2FeP_2O_7$ material can be directly synthesized by solid state method. It has a long cycle life and excellent structural stability because the volume change is only 2.6 % during the charge and discharge process[6]. However, this cathode material can only undergo one-electron reaction, so its theoretical capacity is low, only 97 mAh g^{-1}[7,8].

The $Na_4Fe_3(PO_4)_2(P_2O_7)$ (NFPP) cathode material is composed of $NaFePO_4$ and $Na_2FeP_2O_7$ in a molar ratio of 1:2. The crystal structure belongs to the orthorhombic system, and the space group is Pn21a [9–11]. The material has the advantages of both $NaFePO_4$ and $Na_2FeP_2O_7$, and the theoretical specific capacity is as high as 129 mAh g^{-1} at an average operating voltage of 3.1 V [12]. NFPP is composed of FeO_6 octahedron, PO_4 tetrahedron and P_2O_7 double tetrahedron (pyrophosphate). The crystal structure is shown in Figure 1. Among them, PO_4 and P_2O_7 form a cross-linked three-dimensional channel through a rigid channel constructed by oxygen atoms. Sodium ions can migrate in multiple directions and significantly reduce the diffusion resistance[13,14]. In addition, the PO_4^{3-} and $P_2O_7^{4-}$ dimers in the crystal structure can reduce rotation and distortion, and the volume change of sodium ions during the extraction and insertion process is small, which improves the cycle life of the material[15,16]. At the same time, the material realizes the reversible deintercalation of sodium ions in the three-dimensional sodium ion transport channel through the Fe^{2+}/ Fe^{3+} redox reaction[17]. However, the insulation and steric hindrance of the PO_4^{3-} group lead to low electronic conductivity, which restricts its electrochemical

ISSN 2616-5880 Vol. 6, Issue 3: 30-37, DOI: 10.25236/AJMC.2025.060303

performance[18,19].

To solve this problem, the construction of high conductive matrix is an effective strategy to improve the electrochemical performance of NFPP cathode materials. Wang[20] et al. prepared $Na_4Fe_{2.94}Al_{0.04}(PO_4)_2(P_2O_7)$/C composite cathode material by aluminum doping. Studies have shown that by slightly replacing the Fe^{2+} sites of NFPP with Al^{3+}, Fe defects are introduced into the structure, which not only inhibits the formation of $NaFePO_4$ impurity phase, but also significantly enhances the sodium ion diffusion rate and electronic conductivity Cao[21] et al. prepared $Na_4Fe_3(PO_4)_2(P_2O_7)$ nanospheres with multi-walled carbon nanotubes (MCNTs) as the substrate by spray drying method. This material not only exhibits high electronic conductivity, but also effectively alleviates the structural stress during charging and discharging. Li[22] et al.prepared a high-performance $Na_4Fe_{2.7}Mn_{0.3}(PO_4)_2(P_2O_7)$/rGO composite cathode material by partially replacing Fe^{2+} with Mn^{2+} and combining the double modification method of graphene coating modification. Studies have shown that this modification method not only effectively reduces the diffusion energy barrier of sodium ions, but also reduces the band gap of the material, thereby synergistically enhancing the transmission rate and electronic conductivity of sodium ions.

Although these methods are effective, their complex preparation process and high cost limit large-scale commercial applications. In this paper, NFPP-B cathode materials were prepared by doping with different boron contents by a simple high temperature solid phase method. It is found that the isoelectronic substitution of PO_4^{3-} by small-sized BO_3^{3-} leads to a local lattice shrinkage effect, which not only effectively alleviates the volume change caused by the deintercalation of sodium ions, but also enhances the stability of the three-dimensional framework, thereby significantly improving the electrochemical performance of the material[23]. Since the electronegativity of borate (2.04) is lower than that of phosphate (2.19), the addition of BO_3^{3-} effectively reduces the electron binding energy of Fe^{2+} / Fe^{3+} and reduces the lattice distortion during the redox reaction, thus significantly improving the structural stability of NFPP materials.

An appropriate amount of B doping can improve the reversible specific capacity of NFPP materials, and can also improve the rate performance and cycle performance of the materials. The electrochemical test results show that the NFPP-B0.05 / C material has the best electrochemical performance. The first discharge specific capacity reaches 100.9 mAh g^{-1} at 0.2 C. At an ultra-high rate of 20 C, the discharge specific capacity of 84.1 mAh g^{-1} is still maintained, and the capacity retention rate of 1000 cycles at a high rate of 5 C is 92.6 %. In addition, B doping can also reduce the interface impedance and optimize the sodium ion transmission channel of NFPP material, and improve the ionic conductivity of the material.

2. Experiment Content

2.1 Sample Preparation

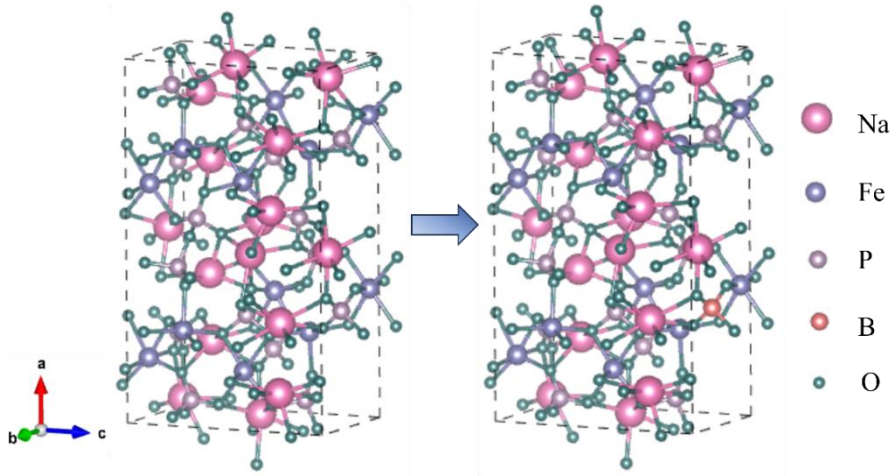

Figure 1 The crystal structure diagram of undoped NFPP cathode material and boron doped NFPP cathode material.

$Na_4Fe_3(PO_4)_{2-x}(P_2O_7)(BO_3)_x$ (NFPP-B) samples were prepared by high temperature solid-state method. Firstly, $Na_4P_2O_7$ (2 mmol), FeC_2O_4 (6 mmol, $NH_4H_2PO_4$ (2-x mmol), H_3BO_3 (x mmol) and citric acid were added to the agate jar in turn, and an appropriate amount of anhydrous ethanol was added as a dispersant. The weight ratio of the material to the agate ball was 1:6. After ball milling for 3 h, the mixture

ISSN 2616-5880 Vol. 6, Issue 3: 30-37, DOI: 10.25236/AJMC.2025.060303

was placed in a vacuum drying oven at 80 ℃ for 8 h. Finally, in an argon atmosphere, the mixture was pretreated at 300 ℃ for 3 h, and then annealed at 550 ℃ for 10 h. The heating rate was 5 ℃ min^{-1}. It is advisable to keep all the given values. In this paper, $Na_4Fe_3(PO_4)_2(P_2O_7)$/C (NFPP/C), $Na_4Fe_3(PO_4)_{1.975}(P_2O_7)(BO_3)_{0.025}$/C (NFPP-B0.025/C), $Na_4Fe_3(PO_4)_{1.95}(P_2O_7)(BO_3)_{0.05}$/C (NFPP-B0.05/C), $Na_4Fe_3(PO_4)_{1.925}(P_2O_7)(BO_3)_{0.075}$/C (NFPP-B0.075/C) were prepared by controlling the stoichiometric ratio of $NH_4H_2PO_4$ and H_3BO_3. The crystal structure before and after doping is shown in Figure 1.

2.2 Material Characterization

The crystal structure of the cathode material powder sample was studied by powder X-ray diffraction (XRD) analysis using a Bruker D8 Advance diffractometer. The microstructure and morphology of the samples were analyzed by scanning electron microscopy (SEM) of the SUPRA 55 sapphire model. The distribution of elements in the samples was observed by X-ray energy dispersive spectrometer (EDS).

2.3 Electrochemical Test

The active material (70 wt %), conductive carbon black (20 wt %) and polyvinylidene fluoride (PVDF, 10 wt %) were fully mixed and added to the above mixture with n-methyl-2-pyrrolidone (NMP) as solvent to prepare slurry. The slurry was evenly coated on the surface of the aluminum foil with a scraper, and then the electrode was dried in a vacuum oven at 80 ℃ for 12 h. After the electrode was dried, the electrode was punched into the required size. The button battery was assembled in a glove box filled with argon, and the assembled battery was tested after standing for 6-12 h at room temperature. The NEWARE system was used to test the charge and discharge performance of the battery under the voltage window of 1.5 ~ 4.5 V. Cyclic voltammetry (CV) and electrochemical impedance spectroscopy (EIS) tests were performed using an electrochemical workstation (Shanghai Chenhua CHI760E).

3. Result and Discussion

In order to determine the composition and crystal structure of the prepared samples, the materials were tested by XRD. Figure.2 shows the powder XRD patterns of NFPP/C, NFPP-B0.025/C, NFPP-B0.05/C and NFPP-B0.075/C after calcination at 550 ℃ for 10 h. Through the analysis of XRD patterns by Highscore, it is found that the diffraction points of all samples are orthorhombic. It can be seen from the figure that the diffraction peaks of NFPP/C, NFPP-B0.025/C and NFPP-B0.05/C all correspond to the standard card PDF # 92-023-6316 one by one, and no other diffraction peaks are observed, indicating that these two samples have high purity and no other impurity phases appear, which indicates that the appropriate amount of B element doping does not destroy the crystal structure of NFPP materials. Among them, the NFPP-B0.05/C sample has the highest diffraction peak intensity and good crystallinity. However, the peak intensity of the NFPP-B0.075/C sample is very low, which may be due to excessive B doping interferes with the crystal growth of the NFPP material. The disordering of the lattice arrangement reduces the crystallinity of the material, and the amorphous region cannot produce sharp diffraction peaks, resulting in a decrease in the intensity of the main peak.

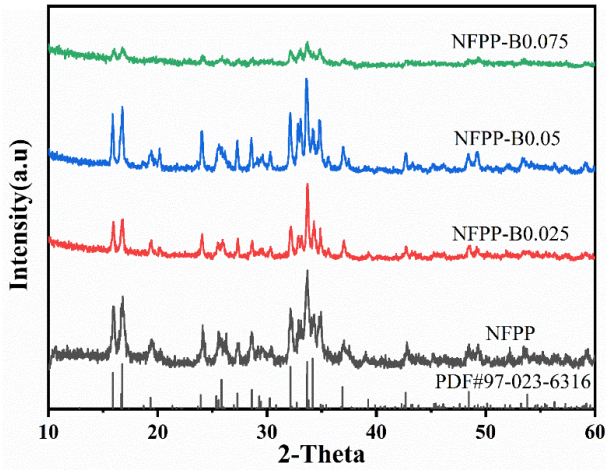

Figure 2 XRD patterns of NFPP/C, NFPP-B0.025/C, NFPP-B0.05/C, and NFPP-B0.075/C

The morphologies of NFPP/C, NFPP-B0.025/C, NFPP-B0.05/C and NFPP-B0.075/C were analyzed

ISSN 2616-5880 Vol. 6, Issue 3: 30-37, DOI: 10.25236/AJMC.2025.060303

by SEM, as shown in Figure 3. The particles of the NFPP/C sample in Figure 3 (a) are densely arranged, and there are large pores in the local area. Such unevenly distributed large pores may cause local polarization. The NFPP-B0.025/C and NFPP-B0.05/C samples in Figure 3 (b) and (c) show irregular granular structure with a small size of about 200 nm-600 nm. The overall distribution is uniform and there is no obvious agglomeration. In addition, there is also a small pore structure, which is beneficial to alleviate the volume expansion of the battery during charge and discharge and improve the cycle life of the material. The size of NFPP-B0.075/C sample in Figure 3 (d) varies greatly, which may be caused by lattice defects caused by excessive B doping.

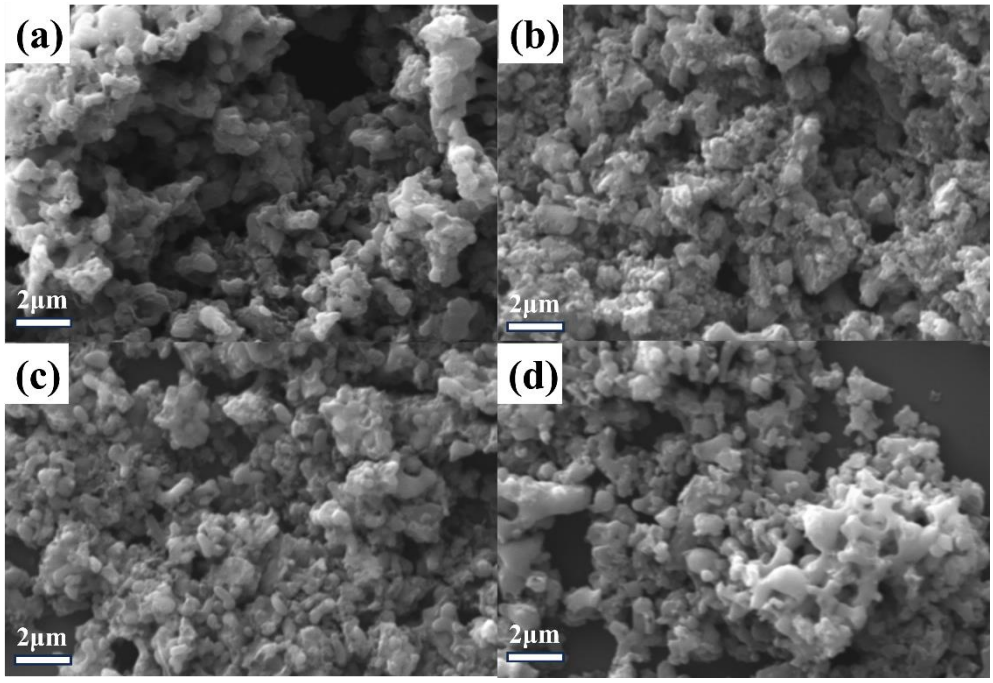

Figure 3 SEM images of (a)NFPP/C, (b)NFPP-B0.025/C, (c)NFPP-B0.05/C, and (d)NFPP-B0.075/C

The distribution of various elements in NFPP-B0.05 / C samples was analyzed by energy dispersive X-ray spectroscopy (EDS), as shown in Figure 4. It can be clearly seen from the diagram that Na, Fe, P, O, B and C elements are evenly distributed in the NFPP-B0.05 / C sample.

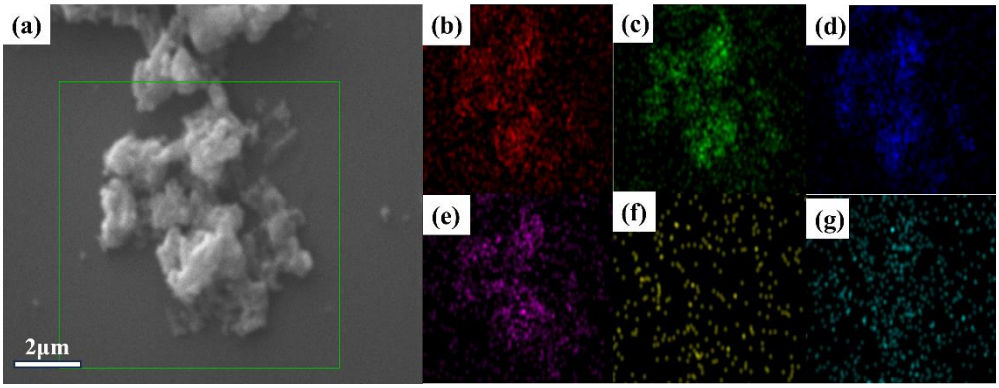

Figure 4 EDS diagram of NFPP-B0.05/C sample: (a)SEM, (b)Na, (c) Fe, (d)P, (e)O, (f)B, (g)C

The electrochemical properties of NFPP/C, NFPP-B0.025/C, NFPP-B0.05/C and NFPP-B0.075/C were analyzed by charge-discharge test, as shown in Figure 5. Figure 5 (a) is the rate performance of the four samples at 0.2 C, 0.5 C, 1 C, 2 C, 5 C, 10 C and 20 C, respectively. Figure 5 (b) is the first charge-discharge curve of the four samples. It can be clearly seen from the diagram that the initial discharge specific capacity of the NFPP-B0.05/C sample is the highest, which is 100.9 mAh g^{-1}. With the increase of the rate, the specific capacity of the four samples shows different degrees of attenuation. Among them, the NFPP-B0.05/C sample has the best rate performance in all samples. When the rate increases to 20 C, the sample still maintains a discharge specific capacity of 84.1 mAh g^{-1}. In contrast, the NFPP-B0.075/C sample has the worst rate performance and the largest attenuation. This phenomenon may be due to the

ISSN 2616-5880 Vol. 6, Issue 3: 30-37, DOI: 10.25236/AJMC.2025.060303

lattice distortion effect caused by excessive boron doping. This structural change significantly increases the migration energy barrier of sodium ions. It can be seen from the first charge-discharge curves in Figure 5 (b) that the double voltage platforms appear in the charge / discharge process of the four samples, which are due to the step-by-step deintercalation of multi-sodium sites and the step-by-step redox reaction of Fe^{2+}/ Fe^{3+}.

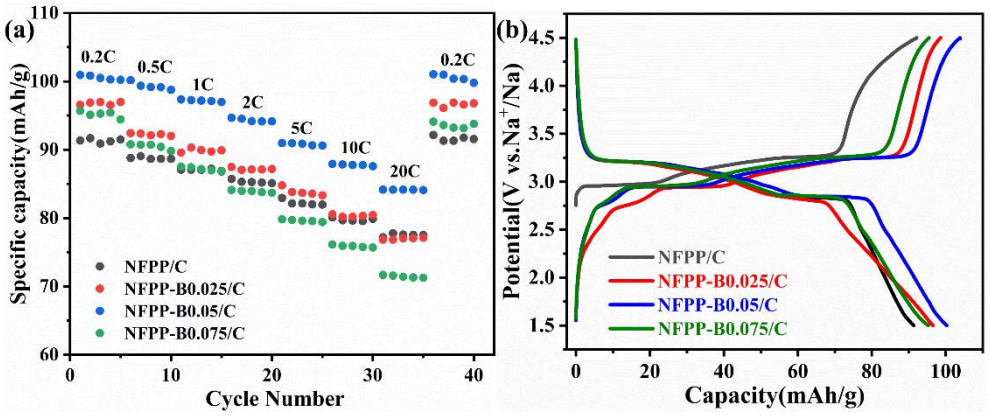

Figure 5 The (a) rate performance and (b) charge-discharge curve at 0.2 C of NFPP/C, NFPP-B0.025/C, NFPP-B0.05/C and NFPP-B0.075/C samples

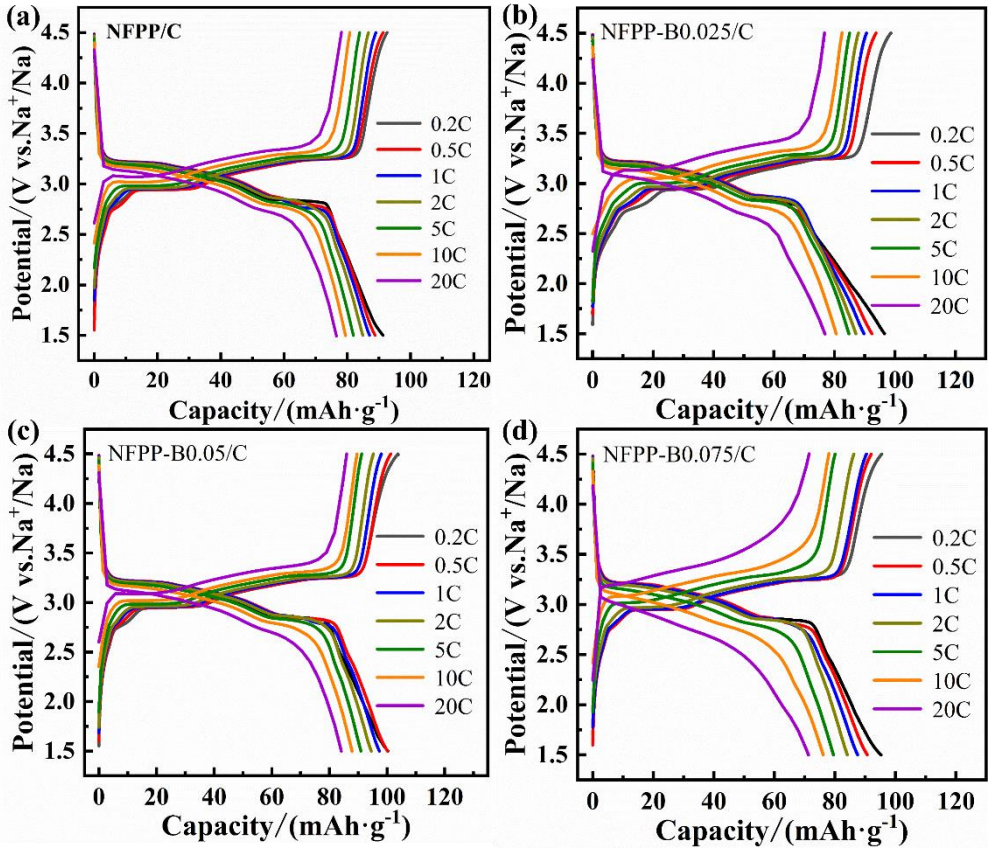

Figure 6 The charge-discharge curves of (a) NFPP/C, (b) NFPP-B0.02/C, (c) NFPP-B0.05/C, and (d) NFPP-B0.075/C at different rates.

According to the test results of different rates, the charge and discharge behaviors of NFPP/C, NFPP-B0.025/C, NFPP-B0.05/C and NFPP-B0.075/C samples at different rates were analyzed, as shown in Figure 6. It can be seen from the graph that all samples show a flat charge-discharge platform at low rates (0.2 C ~ 1 C), indicating that the process of sodium ion extraction / insertion in the lattice is highly reversible during charge-discharge. The charge-discharge platform of NFPP-B0.05/C sample is the widest and flatest, indicating that the crystal structure stability of the sample is the best. At a high rate of 20 C, the discharge specific capacities of the four samples are 77.2 mAh g^{-1}, 77.8 mAh g^{-1}, 84.1 mAh g^{-}

ISSN 2616-5880 Vol. 6, Issue 3: 30-37, DOI: 10.25236/AJMC.2025.060303

[1] and 71.7 mAh g^{-1}, respectively. The NFPP-B0.05/C sample has the highest discharge specific capacity, which indicates that an appropriate amount of B doping can improve the electronic conductivity and sodium ion diffusion rate. In addition, the polarization voltage of NFPP-B0.05/C is the smallest among the four samples, indicating that an appropriate amount of B element doping can reduce the sodium ion migration energy barrier.

In addition, the cycling performance of NFPP / C and NFPP-B0.05 / C samples was analyzed after 1000 cycles at 5 C, as shown in Figure 7. It can be seen from the figure that the capacity of the NFPP/C sample decays rapidly, from the initial 81.9 mAh g^{-1} to 68.1 mAh g^{-1}, the capacity retention rate is only 74.5 %, and the average decay rate is 0.0255 %. The capacity decay of the NFPP-B0.05/C sample is relatively slow, and the initial specific capacity is 88.6 mAh g^{-1}. After 1000 cycles, the specific capacity is still 82 mAh g^{-1}, the capacity retention rate is 92.6 %, and the average decay rate is only 0.0074 %. It is verified again that an appropriate amount of B element doping can improve the cycle stability of NFPP materials.

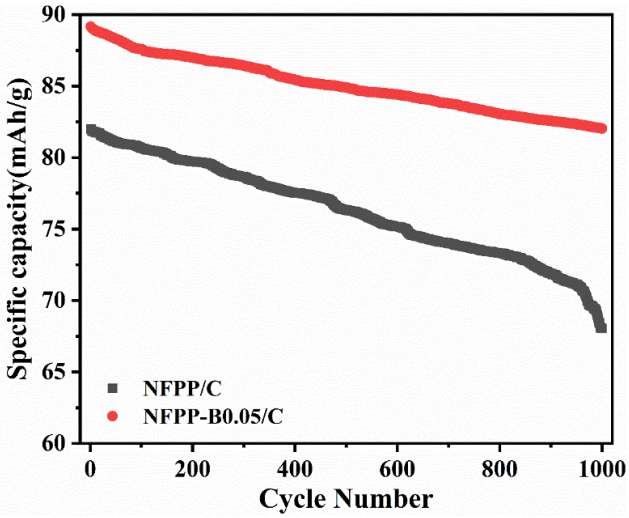

Figure 7 Cyclic performance of NFPP/C and NFPP-B0.05/C samples at 5 C

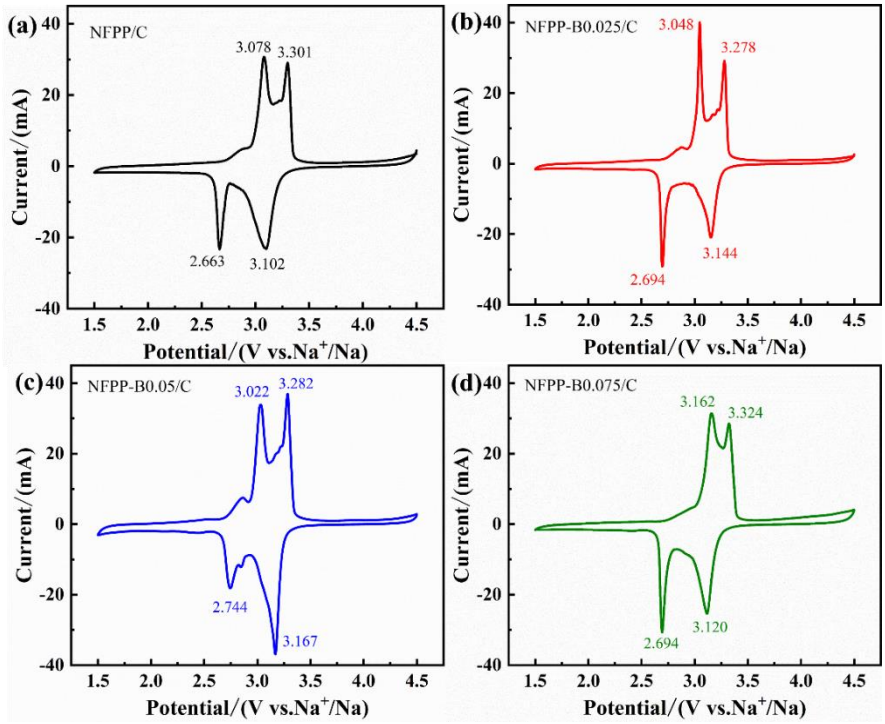

Figure 8 CV curves of (a) NFPP/C, (b) NFPP-B0.02 /C, (c) NFPP-B0.05/C, and (d) NFPP-B0.075/C at a scan rate of 0.2 mV s-1

In this chapter, the electrochemical properties of NFPP/C, NFPP-B0.025/C, NFPP-B0.05/C and

ISSN 2616-5880 Vol. 6, Issue 3: 30-37, DOI: 10.25236/AJMC.2025.060303

NFPP-B0.075/C were tested by cyclic voltammetry. The test voltage range is 1.5 ~ 4.5 V, and the scanning rate is 0.2 mV s^{-1}, as shown in Figure 8. It can be seen from the figure that all the samples have two pairs of sharp redox peaks, which also corresponds to the dual voltage platform of the first charge-discharge curves of the four samples in Figure 6 (b), indicating that all the samples have good electrochemical performance. In addition, NFPP-B0.025/C and NFPP-B0.05/C samples showed multiple weak redox peaks in the range of 3.0-3.2 V, reflecting the step-by-step deintercalation process of sodium ions at different lattice sites in the material.

In order to better understand the ion diffusion kinetics of NFPP/C, NFPP-B0.025/C, NFPP-B0.05/C and NFPP-B0.075/C samples, electrochemical impedance spectroscopy was used to analyze the ion diffusion kinetics of NFPP/C, NFPP-B0.025/C, NFPP-B0.05/C and NFPP-B0.075/C. As shown in figure 9, the insertion part in the figure is the equivalent circuit model. Figure 9 (a) is the Nyquist diagram of four samples. It can be seen from the diagram that the Nyquist diagram of all samples consists of a semicircle (high frequency region) and an oblique line (low frequency region), corresponding to charge transfer resistance (Rct) and Warburg impedance (Zw), respectively. The Rct values of the four samples were 605.65 Ω, 510.11 Ω, 168.18 Ω and 755.07 Ω, respectively. The Rct value of NFPP-B0.05 / C sample was much smaller than that of the other three samples, indicating that the charge transfer ability of the sample was the best.

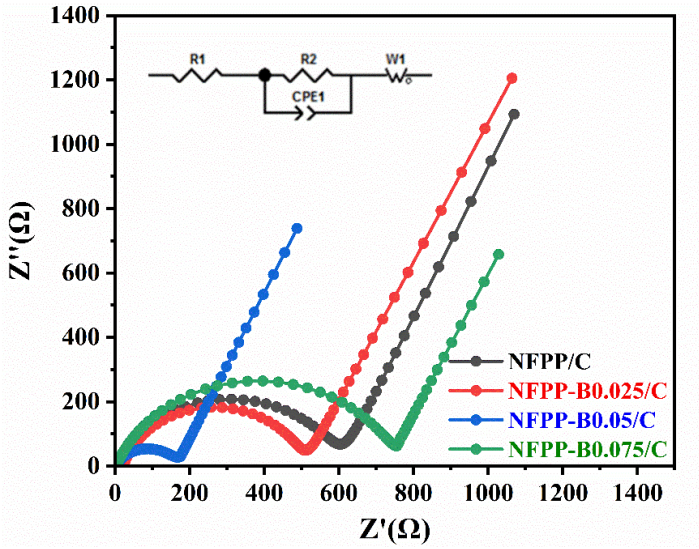

Figure 9 Nyquist plots of NFPP/C, NFPP-B0.025/C, NFPP-B0.05/C and NFPP-B0.075/C

4. Conclusions

In summary, the study of B element doping in NFPP cathode materials shows that the use of small-sized BO_3^{3-} doping instead of PO_4^{3-} in NFPP materials can effectively induce local lattice shrinkage. This microstructure change is of great significance for improving the overall performance of the material. Specifically, the local lattice shrinkage can significantly reduce the volume expansion problem caused by the detachment and embedding of sodium ions during charge and discharge. This improvement not only helps to optimize the stability of the three-dimensional framework, but also effectively alleviates the volume change stress during the sodium ion deintercalation process, thereby enhancing the electrochemical performance of the material. An appropriate amount of B doping can improve the reversible specific capacity of NFPP materials, and can also improve the rate performance and cycle performance of the materials. The electrochemical test results show that the NFPP-B0.05/C material has the best electrochemical performance. The discharge specific capacity reaches 100.9 mAh g^{-1} at 0.2 C. At an ultra-high rate of 20 C, the discharge specific capacity of 84.1 mAh g^{-1} is still maintained, and the capacity retention rate is 92.6 % after 1000 cycles at a high rate of 5 C. In addition, it can also reduce the interface impedance and optimize the sodium ion transport channel of the NFPP material to improve the ionic conductivity of the material.

References

[1] YUE P. Introduction of LFP and Ternary Cathode Materials of Lithium Battery[J]. Highlights in

ISSN 2616-5880 Vol. 6, Issue 3: 30-37, DOI: 10.25236/AJMC.2025.060303

Science, Engineering and Technology, 2023, 58: 387-394.
[2] KIM J, SEO D H, KIM H, et al. Unexpected discovery of low-cost maricite NaFePO4 as a high-performance electrode for Na-ion batteries[J]. Energy & Environmental Science, 2015, 8(2): 540-545.
[3] JIANG N, WANG X, ZHOU H, et al. Achieving Fast and Stable Sodium Storage in Na4Fe3(PO4)2(P2O7) via Entropy Engineering[J]. Small, 2024: 2308681.
[4] LIU B, ZHANG Q, LI L, et al. Achieving highly electrochemically active maricite NaFePO4 with ultrafine NaFePO4@C subunits for high rate and low temperature sodium-ion batteries[J]. Chemical Engineering Journal, 2021, 405: 126689.
[5] ÖZDOGRU B, DYKES H, GREGORY D, et al. Elucidating cycling rate-dependent electrochemical strains in sodium iron phosphate cathodes for Na-ion batteries[J]. Journal of Power Sources, 2021, 507: 230297.
[6] XIONG F, LI J, ZUO C, et al. Mg-Doped Na4Fe3(PO4)2(P2O7)/C Composite with Enhanced Intercalation Pseudocapacitance for Ultra-Stable and High-Rate Sodium-Ion Storage[J]. Advanced Functional Materials, 2023, 33(6): 2211257.
[7] TANG W, SONG X, DU Y, et al. High-performance NaFePO4 formed by aqueous ion-exchange and its mechanism for advanced sodium ion batteries[J]. Journal of Materials Chemistry A, 2016, 4(13): 4882-4892.
[8] XIONG F, AN Q, XIA L, et al. Revealing the atomistic origin of the disorder-enhanced Na-storage performance in NaFePO4 battery cathode[J]. Nano Energy, 2019, 57: 608-615.
[9] XIN Y, WANG Q, WANG Y, et al. Experimental and theoretical investigation of cobalt and manganese substitution in Na4Fe3(PO4)2P2O7 as a high energy density cathode material for sodium-ion batteries[J]. Chemical Engineering Journal, 2024, 483: 149438.
[10] PU X, WANG H, YUAN T, et al. Na4Fe3(PO4)2(P2O7) nanospheres as low-cost, high-performance cathode material for sodium-ion batteries[J]. Energy Storage Materials, 2019, 22: 330-336.
[11] KOSOVA N V, BELOTSERKOVSKY V A. Sodium and mixed sodium/lithium iron ortho-pyrophosphates: Synthesis, structure and electrochemical properties[J]. Electrochimica Acta, 2018, 278: 182-195.
[12] KOSOVA, SHINDROV. Effect of Mixed Li+/Na+-ion Electrolyte on Electrochemical Performance of Na4Fe3(PO4)2(P2O7) in Hybrid Batteries[J]. Batteries, 2019, 5(2): 39.
[13] CHEN M, HUA W, XIAO J, et al. NASICON-type air-stable and all-climate cathode for sodium-ion batteries with low cost and high-power density[J]. Nature Communications, 2019, 10(1): 1480.
[14] CHEN Y, DONG C, CHEN L, et al. "One stone two birds" design for hollow spherical Na4Fe3(PO4)2P2O7/C cathode enabled high-performance sodium-ion batteries from iron rust[J]. EcoMat, 2023, 5(10): e12393.
[15] ZHANG J, TANG L, ZHANG Y, et al. Polyvinylpyrrolidone assisted synthesized ultra-small Na4Fe3(PO4)2(P2O7) particles embedded in 1D carbon nanoribbons with enhanced room and low temperature sodium storage performance[J]. Journal of Power Sources, 2021, 498: 229907.
[16] GE X, HE L, GUAN C, et al. Anion Substitution Strategy toward an Advanced NASICON-$Na_4Fe_3(PO_4)_2P_2O_7$ Cathode for Sodium-Ion Batteries[J]. ACS Nano, 2024, 18(2): 1714-1723.
[17] WEN R, MULAN Q, YIFAN Z, et al. Electrospun Na4Fe3(PO4)2(P2O7) nanofibers as free-standing cathodes for ultralong-life and high-rate sodium-ion batteries[J/OL]. Energy Storage Materials, 2023, 54: 776-783.
[18] DONG C, TANG S, CHEN Y, et al. Identifying the Synergistic Na+/Zn2+ Co-Intercalation Mechanism for Boosting Electrochemical Performance of Na4Fe3(PO4)2(P2O7) in Zn-ion Batteries[J]. ACS Materials Lett, 2023, 5(4): 1170-1178.
[19] GAO J, TIAN Y, MEI Y, et al. Robust NASICON-type iron-based Na4Fe3(PO4)2(P2O7) cathode for high temperature sodium-ion batteries[J]. Chemical Engineering Journal, 2023, 458: 141385.
[20] WANG Y, FEI W, ZHANG X, et al. Rapid mechanochemical synthesis of high-performance Na4Fe2.94Al0.04(PO4)2(P2O7)/C cathode material for sodium-ion storage[J]. Journal of Colloid and Interface Science, 2024, 664: 220-227.
[21] CAO Y, XIA X, LIU Y, et al. Scalable synthesizing nanospherical Na4Fe3(PO4)2(P2O7) growing on MCNTs as a high-performance cathode material for sodium-ion batteries[J]. Journal of Power Sources, 2020, 461: 228130.
[22] XIAOQIANG L, YU Z, BOLUN Z, et al. Mn-doped Na4Fe3(PO4)2(P2O7) facilitating Na+ migration at low temperature as a high-performance cathode material of sodium ion batteries[J/OL]. Journal of Power Sources, 2022, 521: 230922.
[23] ZAINURI M, TRIWIKANTORO, ZAHRA P A. Active Materials LiFeSixP1-xO4/C as Lithium-Ion Battery Cathode with Doping Variations Si Ions (0≤x≤0,06)[J]. Key Engineering Materials, 2020, 860: 75-80.